The Astrophysical Journal Supplement Series, 283:13 (10pp), 2026 March https://doi.org/10.3847/1538-4365/ae39c7

POLAMI Multiwavelength Polarization Study of Active Galactic Nuclei Jets: A Millimeter–Optical Comparison

Carolina Casadio[1,2], Dmitry Blinov[1,2], Iván Agudo[3], Ioannis Myserlis[4], Clemens Thum[4], Svetlana Jorstad[5,6], Alan Marscher[5], Haocheng Zhang[7,8], Juan Escudero Pedrosa[3,9], Diego Álvarez-Ortega[1,2], Zachary R. Weaver[5], Manasvita Joshi[10], Callum McCall[11], Helen Jermak[11], Iain A. Steele[11], George A. Borman[12], Tatiana S. Grishina[6], Elena G. Larionova[6], Daria A. Morozova[6], Sergey S. Savchenko[6,13], Ivan S. Troitskiy[6], Yulia V. Troitskaya[6], and Andrey A. Vasilyev[6]

[1] Institute of Astrophysics, Foundation for Research and Technology-Hellas, GR-70013 Heraklion, Greece; ccasadio@ia.forth.gr, blinov@physics.uoc.gr
[2] Department of Physics, University of Crete, GR-70013, Heraklion, Greece
[3] Instituto de Astrofísica de Andalucía-CSIC, Glorieta de la Astronomía s/n, 18008 Granada, Spain
[4] Institut de Radioastronomie Millimétrique, Avenida Divina Pastora, 7, Local 20, E-18012 Granada, Spain
[5] Institute for Astrophysical Research, Boston University, 725 Commonwealth Avenue, Boston, MA 02215, USA
[6] Saint Petersburg State University, 7/9 Universitetskaya nab., St. Petersburg, 199034, Russia
[7] University of Maryland, Baltimore County, Baltimore, MD 21250, USA
[8] NASA Goddard Space Flight Center, Greenbelt, MD 20771, USA
[9] Center for Astrophysics | Harvard & Smithsonian, Cambridge, MA 02138, USA
[10] FAS Research Computing, Harvard University, 38 Oxford Street, Cambridge, MA 02138, USA
[11] Astrophysics Research Institute, Liverpool John Moores University, Liverpool Science Park IC 2, 146 Brownlow Hill, Liverpool L3 5RF, UK
[12] Crimean Astrophysical Observatory RAS, P/O Nauchny, 298409, Crimea[†]
[13] Pulkovo Observatory, St. Petersburg, 196140, Russia
Received 2025 December 16; accepted 2026 January 14; published 2026 February 18

Abstract

Millimeter-band polarimetry offers a powerful probe of active galactic nuclei jets, accessing regions less affected by opacity and Faraday rotation than at longer radio wavelengths. As part of the POLAMI program, we have conducted 14 yr of 1 and 3 mm polarization monitoring of a sample of gamma-ray-bright blazars with the IRAM 30 m telescope, complemented here with long-term optical polarimetric observations from multiple facilities. We aim to test whether current models of parsec-scale jet physics are consistent with observed multiband polarization behavior. Using a Bayesian framework, we derive intrinsic mean flux densities and modulation indices for total flux and fractional polarization, and characterize electric vector position angle (EVPA) variability using circular statistics. We then examine how these quantities reflecting variability properties across millimeter and optical bands relate to synchrotron peak frequency, jet orientation, and radio/gamma-ray luminosities. BL Lacertae (BL Lac) objects exhibit, on average, higher fractional polarization and lower EVPA variability than flat-spectrum radio quasars (FSRQs) at all wavelengths. Fractional polarization increases with frequency, consistent with increasingly ordered magnetic fields at shorter wavelengths. BL Lacs also show more frequent alignment of EVPAs between optical and millimeter bands, whereas FSRQs display weaker coherence. EVPA variability correlates positively with radio and gamma-ray luminosities and negatively with synchrotron peak frequency, most strongly in the optical. We further find a positive correlation between EVPA spread and fractional polarization variability, suggesting a direct link between magnetic-field structure and polarization dynamics.

Unified Astronomy Thesaurus concepts: Active galaxies (17); Blazars (164); Radio continuum emission (1340); Polarimetry (1278); Flat-spectrum radio quasars (2163); BL Lacertae objects (158)

Materials only available in the online version of record: figure set

1. Introduction

Relativistic jets in active galactic nuclei (AGN) are considered Poynting-flux-dominated at their origin, with strong magnetic fields that influence the jet flow dynamics and particle acceleration (R. D. Blandford & R. L. Znajek 1977; J. C. McKinney 2006). Linear polarization studies at short millimeter wavelengths and optical frequencies, where the emission is believed to be optically thin and, therefore, free of opacity effects, are fundamental to investigating the behavior and, consequently, the role of magnetic fields in jets.

Blazars are a subset of radio-loud AGN characterized by powerful relativistic jets that are closely aligned with our line of sight (e.g., P. Padovani et al. 2017). They are typically classified into flat-spectrum radio quasars (FSRQs) if they display strong, broad, and narrow emission lines in their optical spectra, and BL Lacertae objects (BL Lacs) if they show weak or no emission lines (C. M. Urry & P. Padovani 1995). The bulk jet motion, coupled with the small viewing angle, results in Doppler boosting, which amplifies the jet's brightness and shortens observed variability timescales.

While the millimeter-wave emission in blazars is expected to be dominated by synchrotron radiation from the relativistic jet, optical emission can have multiple production mechanisms (synchrotron,

[†] While the AAS journals adhere to and respect UN resolutions regarding the designations of territories (available at http://www.un.org/press/en), it is our policy to use the affiliations provided by our authors on published articles.

thermal emission, or recombination lines emission) and locations (accretion disk, broad line region (BLR), or jet) (S. A. Podjed et al. 2024). Linear polarization studies can help distinguish between all these possible scenarios. Synchrotron emission from beamed jets is expected to exhibit a variable degree of polarization, ranging from a few to several tens of percent. A strong contribution from either the unbeamed synchrotron components or the thermal components, like the accretion disk, BLR, or torus, can lower the fractional polarization to less than a few percent (M. Böttcher et al. 2017). At the same time, these components are expected to reduce the variability in the combined emission's total flux and polarization.

I. Agudo et al. (2018b) presented the Polarimetric Monitoring of AGN at Millimetre Wavelengths (POLAMI) program for the study of the polarimetric properties of a sample of radio and gamma-ray-bright blazars and radio galaxies with the IRAM 30 m telescope at 3.5 and 1.3 mm, and biweekly (on average) cadence. New important results on polarization variability in POLAMI sources were presented in I. Agudo et al. (2018a), namely: (i) the fractional polarization at 1 mm is found to be higher, more variable, and to vary faster than at 3 mm; (ii) the linear polarization angle is, in general, highly variable, and the 1 mm variations seem to be faster than those at 3 mm. Faster variability and larger amplitudes at 1 mm than at 3 mm are also seen in total flux density.

I. Agudo et al. (2018a) confirmed that opacity effects are not the dominant cause behind the variability observed at millimeter wavelengths. In general, sources are optically thin at both 1 and 3 mm, becoming optically thick at 3 mm only during certain prominent flares and for periods shorter than the flaring state duration. POLAMI's results support a multizone model in which 1 mm emission originates in more compact regions with better-ordered magnetic fields than at 3 mm, as predicted by the turbulent extreme multizone model, where turbulence drives the variability of jet emission (A. P. Marscher 2014). A certain degree of magnetic-field disorder is required to explain the relatively low fractional polarization observed, which is consistently far below the theoretical maximum (∼70%; A. G. Pacholczyk 1970) for synchrotron radiation in a uniform field. However, the frequent alignment between the linear polarization angle at optical frequencies and those of the radio core (A. P. Marscher & S. G. Jorstad 2021) or stationary jet features (M. Sasada et al. 2018) indicates that an ordered magnetic-field component must also be present. Pure turbulence alone cannot even explain the systematic rotations observed in the optical linear polarization vectors of some blazars (D. Blinov et al. 2018, 2021a).

This work presents a systematic comparative study of optical and millimeter-wavelength polarimetric observations of a sample of blazars. Our goal is to address the long-standing questions concerning the origin of optical emission in blazars and the intrinsic physical conditions that differentiate them. For this study, we make use of the long-term POLAMI program for the millimeter data and several optical monitoring programs for the optical data. While this paper concentrates on integrated quantities, a complementary time-dependent variability analysis is currently in preparation.

2. Data and Methods

The priority sample of the POLAMI program, considered in this study, includes 34 sources in total: 21 FSRQs, 11 BL Lacs, and 2 radio galaxies. The list of sources with the associated class is reported in Table 1. POLAMI observations at 1.3 mm (230 GHz) and 3.5 mm (86.24 GHz) were regularly (average sampling ∼20 days) carried out at the IRAM 30 m Telescope in Pico Veleta since 2006 (2009 at 1 mm). Observation strategy and data calibration are described in detail (I. Agudo et al. 2018b). The millimeter radio data were complemented by optical photopolarimetric observations from the following telescopes: (1) the 2.2 m telescope of the Calar Alto Observatory (Almería, Spain);[14] (2) the 2 m Liverpool Telescope of the Observatorio del Roque de Los Muchachos (Canary Islands, Spain); (3) the 1.83 m Perkins Telescope of Lowell Observatory (Flagstaff, USA);[15] (4) the 1.54 and 2.3 m telescopes of Steward Observatory (Mount Bigelow and Kitt Peak, USA);[16] (5) the 70 cm AZT-8 Telescope of the Crimean Astrophysical Observatory; and (6) the 40 cm LX-200 Telescope of St. Petersburg State University (St. Petersburg, Russia). Additional data were obtained from the publicly

Table 1
List of Sources

J2000 Name	Common Name	Opt. Class	References
J0222+4302	3C66a	B	R14
J0238+1636	AO0235+16	B	R14
J0319+4130	3C84	RG	VCV10
J0339-0146	CTA26	Q	R14
J0418+3801	3C111	RG	VCV10
J0423-0120	PKS0420-01	Q	R14
J0530+1331	PKS0528+13	Q	R14
J0721+7120	S50716+71	B	R14
J0738+1742	PKS0735+17	B	R14
J0830+2410	OJ248	Q	R14
J0831+0429	OJ49	B	R14
J0841+7053	Q0836+71	Q	R14
J0854+2006	OJ287	B	R14
J0958+6533	S40954+65	B	R14
J1058+0133	PKS1055+01	Q	R14
J1104+3812	MKN421	B	R14
J1130-1449	PKS1127-14	Q	VCV10
J1159+2914	4C 29.45	Q	R14
J1221+2813	WComae	B	R14
J1224+2122	PKS1222+21	Q	R14
J1229+0203	3C273	Q	R14
J1256-0547	3C279	Q	R14
J1310+3220	B21308+32	Q	R14
J1408-0752	PKS1406-07	Q	R14
J1512-0905	PKS1510-08	Q	R14
J1613+3412	DA 406	Q	R14
J1635+3808	4C 38.41	Q	R14
J1642+3948	3C345	Q	R14
J1733-1304	Q1730-13	Q	R14
J1751+0939	OT081	B	R14
J2202+4216	BLLac	B	R14
J2225-0457	3C446	Q	R14
J2232+1143	CTA102	Q	R14
J2253+1608	3C454.3	Q	R14

Note. Optical classes (B: BL Lac, RG: radio galaxy, and Q: quasar) are taken from J. L. Richards et al. (2014; R14) and M. P. Véron-Cetty & P. Véron (2010; VCV10).

[14] Observations from the Monitoring AGN with the Calar Alto Telescopes (MAPCAT) program; see I. Agudo et al. (2012).
[15] From 2019 the Perkins telescope is Perkins Telescope Observatory (PTO) owned by Boston University.
[16] https://james.as.arizona.edu/~psmith/Fermi/

available RoboPol (D. Blinov et al. 2021b) and Kanata (R. Itoh et al. 2016) monitoring programs, using (7) the 1.3 m telescope of the Skinakas Observatory (Crete, Greece), and (8) the 1.5 m Kanata Telescope at the Higashi-Hiroshima Observatory (Japan). Most of the optical polarimetric data were obtained in the *R* band, with a few exceptions. The Steward Observatory data were collected using the SPOL spectropolarimeter over the 5000–7000 Å range. At the LX-200 telescope, polarimetry was conducted in white light, with an effective bandpass approximately matching the *R* band. For the three sources observed in the Kanata program, *V*-band data were used. In the case of the Liverpool Telescope, RINGO3 polarimetric measurements were derived by averaging the "*f*" and "*e*" bands (D. M. Arnold et al. 2012). Although not all measurements were made strictly in the *R* band, the effective wavelengths are sufficiently close, and optical polarization parameters typically vary only weakly and irregularly with wavelength (A. P. Marscher & S. G. Jorstad 2021). Therefore, these data were treated as equivalent to *R*-band measurements and included in the analysis. For the total optical flux density, we used only photometry obtained in the *R* band, which was corrected for the Galactic extinction using data from E. F. Schlafly & D. P. Finkbeiner (2011). The total flux and fractional polarization were not corrected for host-galaxy emission, as such contributions are negligible for most sources.

POLAMI data at 3 and 1 mm cover the periods from 2006 October to 2021 October and from 2009 December to 2021 October, respectively, corresponding to average total coverages of roughly 14 yr (3 mm) and 11 yr (1 mm). Optical data are collected from 2005 April to 2021 September and cover, on average, 15 yr. The average data sampling per source at 3 mm goes from 17 to 47 days, and from 24 to 146 days at 1 mm. At optical frequencies, the average data sampling per source ranges from intraday scales to 18 days.

We inspected data at all three frequencies and discarded electric vector position angle (EVPA) measurements when $p/\sigma_p < 2.5$, where p is the fractional polarization and σ_p its uncertainty. After excluding unreliable EVPAs, if a source is left with fewer than 20 EVPA measurements at any band, we did not compute the average EVPA value at that band.

To determine the mean flux density and a measure of its variability, we employed the Bayesian approach introduced by J. L. Richards et al. (2011). The intrinsic modulation index quantifies the amplitude of variability in the flux density of a source, independent of observational uncertainties and sampling effects, and is defined as the ratio of the intrinsic standard deviation of the flux density distribution to its intrinsic mean, $m_{\rm fl} = \sigma_S/S_0$, where "intrinsic" refers to the variability that would be observed with perfect sampling and no measurement errors. The Bayesian method from J. L. Richards et al. (2011) allows for the simultaneous estimation of the maximum likelihood values of both S_0 and $m_{\rm fl}$, providing information about the source's intrinsic flux density variability and average flux, deconvolved from both observational errors and the effects of finite sampling.

The approach of J. L. Richards et al. (2011) was extended to polarization measurements in D. Blinov et al. (2016) to characterize the intrinsic average fractional polarization, p_0, and the intrinsic modulation index of the fractional polarization, $m_{\rm pol}$. The intrinsic average fractional polarization, p_0, represents the mean polarization fraction of a source, corrected for observational biases and sampling effects, while $m_{\rm pol}$ quantifies the amplitude of variability in the fractional polarization, independent of measurement uncertainties and sampling limitations, and is defined as the ratio of the intrinsic standard deviation to the intrinsic mean, $m_{\rm pol} = \sigma_p/p_0$. A key advantage of this technique is that, in addition to accounting for measurement uncertainties and sampling effects, it also corrects for polarization bias (e.g., J. E. Vaillancourt 2006).

We modeled the observed dependencies using linear least-squares fits. The significance of the fits was tested by applying the same statistical analysis to bootstrapped data. Bootstrapping was performed by resampling the original dataset both with and without replacement. The procedure was repeated 500 times, and the mean and standard deviation of the fitted slopes were compared with those obtained from the original data. We found that the bootstrapping analysis did not change the significance of the correlations; therefore, we consider the analyzed dataset to be a good representation of the parent population.

3. Results

3.1. Average Quantities: EVPA, Jet Position Angles, and p_0

We test the uniformity of the EVPA distribution using a Kolmogorov–Smirnov (K-S) test. The null hypothesis of EVPAs following a uniform distribution is rejected if the likelihood of data occurring under the null hypothesis (p-value) is lower than 0.05. Based on the K-S test, the majority of sources (68%) exhibit nonuniform distributions in millimeter and optical EVPAs. For sources where the EVPA is not uniformly distributed, we compute the mean value and its associated uncertainty using circular statistics. We then compare these mean EVPA values with the jet position angles (PAs) reported by Z. R. Weaver et al. (2022). It is important to note that a large fraction of sources in this study (38%) have a variable jet PA, based on Z. R. Weaver et al. (2022) classification. We visualize the distribution of EVPAs at the different bands in circular histograms, as shown in Figure 1. The red vector represents the jet PA, while blue and yellow vectors indicate the mean of 3 and 1 mm EVPAs, respectively, and are overlaid on the plot if EVPAs do not follow a uniform distribution. In some sources, the optical and millimeter EVPAs tend to be stable around the mean, with >70% of the measurements confined within ±25° of the mean. In general, the stability around a mean orientation is observed more often in 3 mm EVPAs (six sources: J0854+2006, J0958+6533, J1224+2122, J1229+0203, J1256-0547, and J2202+4216) than at 1 mm (two sources: J0854+2006 and J2202+4216) and optical (four sources). The paucity of sources at 1 mm may reflect both limited data and stronger variability at this wavelength.

The list of sources with EVPAs distributed nonuniformly in at least two observing bands is reported in Table 2. In these sources, we can investigate the alignments of mean EVPA orientations across bands. We notice a general agreement between 1 and 3 mm EVPA orientations. In the majority of BL Lacs (64%), millimeter EVPAs are also closely aligned (within 10°, considering 1σ uncertainty) with optical EVPAs, while this happens in the minority (19%) of FSRQs. The alignment of optical or millimeter EVPAs with the jet PA is observed in almost half of the BL Lac objects, and a small percentage of FSRQs, 14% and 24%, respectively, for the optical and millimeter cases.

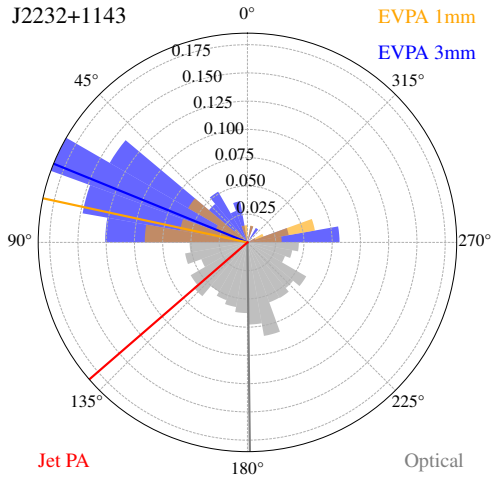

Figure 1. Millimeter (upper hemisphere) and optical (lower hemisphere) EVPA distribution in J2232+1143. EVPA distributions at 3 mm (blue), 1 mm (yellow), and optical (gray) wavelengths are overlaid by vectors of the same color representing the mean value of the respective distribution. A red line marks the jet PA. The different circles mark the counts as a fraction of the total.

(The complete figure set (34 images) is available in the online article.)

In two FSRQs, J1229+0203 and J1613+3412, optical and millimeter EVPAs are almost perpendicular to each other. Interestingly, in both cases, the millimeter EVPAs are also perpendicular to the jet PA, while the optical EVPAs are within 10° of the jet PA.

We computed p_0, as described in Section 2, for all sources and bands, and we found that, in general, the fractional polarization correlates with the observing frequency, with $p_0^{3\,\mathrm{mm}} < p_0^{1\,\mathrm{mm}} < p_0^{\mathrm{optical}}$. Another result is that BL Lac objects have higher average fractional polarization than FSRQs at all bands; the values of p_0 and relative errors are reported in Table 3.

3.2. EVPA Variability

To measure the spread of EVPAs across the different observing bands and object classes, we computed the circular standard deviation of EVPAs per source and frequency. The mean standard deviation values and associated standard errors for the FSRQs and BL Lac object class are reported in Table 4. The mean standard deviation values are higher in FSRQs than in BL Lacs and increase with the observing frequency. However, it is worth noting that all measurements are consistent with each other within 1σ, except for the mean standard deviation of optical EVPAs in FSRQs.

We investigated the dependence of the EVPA standard deviation on the synchrotron peak frequency, ν_{SP} (Figure 2), as well as on the radio (Figure 3), and gamma-ray (Figure 4) luminosities. Here, ν_{SP} refers to the synchrotron peak frequency in the νF_ν spectral energy distribution. Radio and gamma-ray luminosities are taken as proxies of the jet power. The radio monochromatic luminosity at 5 GHz is taken from D. O. Kudryavtsev et al. (2024), while the gamma-ray luminosity was computed using Equation (3) of J. Singal et al. (2014), with energy flux measurements obtained from the Fermi Large Area Telescope Fourth Source Catalog Data Release 4 (S. Abdollahi et al. 2022). Synchrotron peak frequency values in the observer frame are taken from M. Ajello et al. (2020), and redshift measurements are from I. Agudo et al. (2018b). Redshift of J0721+7120 is taken from A. Pichel et al. (2023).

We find an anticorrelation between the EVPA spread and ν_{SP} across all three observing bands, with the strongest correlation observed in the optical data.[17] Given the observed anticorrelations between the synchrotron peak and both jet power and Compton dominance in blazars (G. Ghisellini et al. 1998), we would expect a positive correlation between the EVPA spread and both the radio and gamma-ray luminosities. Such a correlation is indeed found in data: Figures 3 and 4 show the positive correlations between the EVPA standard deviations and the radio and gamma-ray luminosities, which are again stronger in optical data. Only at 1 mm is the best-fit between the EVPA spread and the gamma-ray luminosity consistent with no correlation within 1σ.

From the analysis of EVPA orientations across bands (see Section 3.1), we see that optical EVPAs in FSRQs tend to be less aligned with jet PAs and also with millimeter EVPAs than in BL Lacs. We investigated the possible role of the EVPA variability in leading to the observed differences. We found a positive correlation between the optical EVPA divergences and the optical EVPA spread, as shown in Figure 5. We see that sources with more stable optical EVPAs tend to have optical EVPAs more aligned with both the jet PA and millimeter EVPAs. The majority of BL Lacs and FSRQs are, respectively, located at the left and right ends of the plot in Figure 5.

3.3. Flux Density and Fractional Polarization Variability

We parameterized the variability of the total flux density and fractional polarization using the intrinsic modulation indices m_{fl} and m_{pol}, calculated as described in Section 2. We examined their relationships with the EVPA distribution spread and the intrinsic average fractional polarization p_0.

No correlation was found between EVPA spread and m_{fl}, while m_{pol} positively correlated with the EVPA spread, as shown in Figure 6: the greater the variability in fractional polarization, the broader the range of EVPAs observed.

The intrinsic average fractional polarization p_0 was also analyzed as a function of m_{pol} (Figure 7) and m_{fl} (Figure 8). The outlier in Figure 8 is J2233+1143 (CTA 102), which was excluded from the data fitting. We believe the high m_{fl} in CTA 102 is dominated by the exceptional optical flare it underwent at the end of 2016, during which its brightness increased by 6 magnitudes, making it the most luminous blazar ever observed in the optical sky (C. M. Raiteri et al. 2017).

At optical and 1 mm wavelengths, p_0 showed a negative correlation with m_{pol}, and a positive correlation with m_{fl} in the optical data only. No correlation was found between p_0 and any of the modulation indices at 3 mm. The tendency for sources to exhibit lower p_0 and lower m_{fl} at optical wavelengths may suggest that a turbulent magnetic field dominates at those wave bands. However, a pure turbulence scenario could not account for the p_0–m_{pol} anticorrelation, which instead predicts that a small number of cells leads to both high p_0 and m_{pol} (A. P. Marscher 2014). Another possible explanation could be a different origin for the polarized emission at these frequencies. For example, in some sources, the optical polarized flux may have a significant contribution

[17] Hereafter, we consider a correlation significant when the slope of the best-fit line deviates from zero by more than its 1σ uncertainty.

Table 2
Differences in the Mean EVPA between Bands (Columns (3)–(5)) and between the Mean EVPA in the Three Bands and the Jet PA (Columns (6)–(8))

B1950	J2000	3–1 mm (deg)	3 mm Opt. (deg)	1 mm Opt. (deg)	3 mm PA (deg)	1 mm PA (deg)	Opt. PA (deg)
(1)	(2)	(3)	(4)	(5)	(6)	(7)	(8)
0219+428	J0222+4302	⋯	0.0 ± 2.7	⋯	4.2 ± 6.1	⋯	4.2 ± 5.5
0336−019	J0339−0146	⋯	7.5 ± 4.6	⋯	3.3 ± 6.2	⋯	4.2 ± 5.0
0420−014	J0423−0120	⋯	⋯	27.3 ± 5.7	⋯	44.3 ± 6.4	71.6 ± 4.3
0735+178	J0738+1742	⋯	33.7 ± 5.4	⋯	67.1 ± 11.7	⋯	79.2 ± 11.0
0829+046	J0831+0429	14.6 ± 5.3	16.8 ± 3.0	2.2 ± 4.7	1.7 ± 6.3	12.9 ± 7.3	15.1 ± 5.9
0851+202	J0854+2006	1.0 ± 2.4	5.5 ± 1.5	4.5 ± 2.1	10.3 ± 1.8	11.3 ± 2.3	15.8 ± 1.3
0954+658	J0958+6533	1.0 ± 2.9	8.3 ± 2.1	9.3 ± 2.5	13.8 ± 2.8	14.8 ± 3.1	5.5 ± 2.3
1055+018	J1058+0133	6.8 ± 4.7	74.8 ± 4.3	67.9 ± 4.5	19.0 ± 7.2	25.8 ± 7.4	86.2 ± 7.1
1101+384	J1104+3812	⋯	24.8 ± 4.8	⋯	15.2 ± 15.0	⋯	9.6 ± 14.2
1219+285	J1221+2813	⋯	5.3 ± 4.2	⋯	31.8 ± 11.4	⋯	37.1 ± 10.6
1222+216	J1224+2122	1.6 ± 3.2	1.8 ± 2.0	3.4 ± 2.7	25.5 ± 2.7	27.0 ± 3.2	23.7 ± 2.0
1226+023	J1229+0203	7.1 ± 2.8	89.9 ± 1.6	82.8 ± 2.9	80.5 ± 1.2	87.6 ± 2.7	9.7 ± 1.4
1253−055	J1256−0547	6.0 ± 4.1	18.4 ± 2.6	12.4 ± 3.3	7.4 ± 2.7	13.5 ± 3.4	25.8 ± 1.2
1308+326	J1310+3220	8.1 ± 6.5	23.7 ± 4.8	15.6 ± 6.0	6.4 ± 6.1	1.7 ± 7.1	17.3 ± 5.5
1406−076	J1408−0752	⋯	69.0 ± 6.5	⋯	23.8 ± 8.5	⋯	87.2 ± 8.5
1611+343	J1613+3412	⋯	81.3 ± 4.4	⋯	89.0 ± 5.0	⋯	9.6 ± 4.0
1641+399	J1642+3948	⋯	14.6 ± 2.8	⋯	5.2 ± 3.6	⋯	19.8 ± 2.9
1730−130	J1733−1304	⋯	21.2 ± 5.5	⋯	36.0 ± 4.5	⋯	57.2 ± 3.8
1749+096	J1751+0939	⋯	2.0 ± 4.2	⋯	22.6 ± 4.5	⋯	20.7 ± 2.8
2200+420	J2202+4216	5.1 ± 1.5	0.3 ± 1.0	5.4 ± 1.3	5.6 ± 2.0	0.4 ± 2.2	5.9 ± 1.9
2223−052	J2225−0457	3.5 ± 4.0	68.5 ± 4.1	72.0 ± 4.7	29.8 ± 3.9	33.3 ± 4.6	38.7 ± 4.7
2230+114	J2232+1143	9.9 ± 4.0	67.2 ± 2.5	77.2 ± 3.6	63.0 ± 4.2	53.1 ± 5.0	49.8 ± 3.8
2251+158	J2253+1608	0.8 ± 4.1	47.2 ± 3.0	46.4 ± 3.1	2.3 ± 3.3	1.5 ± 3.4	44.9 ± 1.9

Note. Sources for which the EVPA distribution does not differ significantly from a uniform distribution at two or more frequencies are not listed. All angle differences are given in degrees.

from unbeamed or thermal components, leading to a decrease in fractional polarization below a few percent and resulting in lower flux density variability.

The positive correlation found in optical between p_0 and $m_{\rm fl}$ suggests the tendency for sources to show a high degree of polarization during prominent optical flares. Such a behavior has been occasionally observed in several blazars during single flare events (e.g., A. P. Marscher et al. 2010; C. Casadio et al. 2015).

The lack of correlation between the polarization degree and variability at 3 mm suggests a magnetic-field structure that is less subject to extreme variability. This is confirmed by the 3 mm $m_{\rm pol}$ and $m_{\rm fl}$ values, which are generally lower (<0.7) than the values at 1 mm and optical bands. This is in agreement with the POLAMI results presented in I. Agudo et al. (2018a), where 1 mm data were found to be more variable than 3 mm data both in polarization and total intensity.

Table 3
The Average Intrinsic Mean Fractional Polarization and Its Standard Error for FSRQs and BL Lac Objects at the Three Frequencies

Class	$p_0^{3\ \rm mm}$ (%)	$p_0^{1\ \rm mm}$ (%)	$p_0^{\rm opt}$ (%)
BL Lacs	4.3 ± 0.5	5.9 ± 0.5	9.8 ± 0.8
FSRQs	3.3 ± 0.2	4.7 ± 0.3	7.3 ± 1.0

Table 4
The Mean EVPA Circular Standard Deviations and Associated Standard Errors Computed at the Three Frequencies for FSRQs and BL Lac Objects

Class	Std. 3 mm (deg)	Std. 1 mm (deg)	Std. Opt. (deg)
BL Lacs	33.0 ± 4.6	32.98 ± 6.3	39.8 ± 3.9
FSRQs	37.3 ± 2.6	37.9 ± 2.5	49.4 ± 3.1

4. Discussion

4.1. On the Origin of Optical and Millimeter-wave Emission in Blazars

The comprehensive analysis of optical and millimeter-wave polarimetric data for the 21 FRSQs and 11 BL Lacs monitored under the POLAMI program has revealed class- and frequency-dependent correlations. Some of the reported correlations were also previously found by S. G. Jorstad et al. (2007), who conducted a similar optical–millimeter comparative study on a subsample of the sources considered in this work. Despite the smaller blazar sample (15 sources) and the shorter data coverage ($\leqslant$4 yr) analyzed in S. G. Jorstad et al. (2007), the authors still found that BL Lacs tend to exhibit better alignment of polarization PAs between frequencies and with the jet PA than FSRQs. It is important to note that the results in S. G. Jorstad et al. (2007) are based on single-epoch comparisons, rather than on integrated quantities as in the present study. The fact that blazars exhibit similar behavior on different timescales strengthens the conclusions of the two optical–millimeter comparative studies and highlights the intrinsic differences in magnetic-field configuration and/or emission-site location between the two blazar classes. It is therefore clear that an appropriate physical model of blazars should be able to account for these differences.

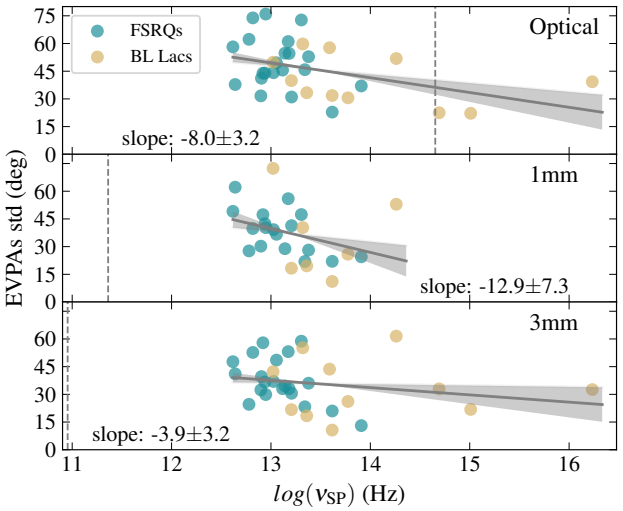

Figure 2. Dependence of the EVPA spread on the synchrotron peak position. The vertical lines in each panel indicate the respective observing frequencies. Notes: the trend observed at 1 and 3 mm, resembling the trend at optical wavelength, is similar to the trend in E. Angelakis et al. (2016) and fits with the model proposed in W. J. Potter & G. Cotter (2015). The gray line and the shadow area represent the best linear fit using a least-squares fitting method and the 1σ deviation, respectively.

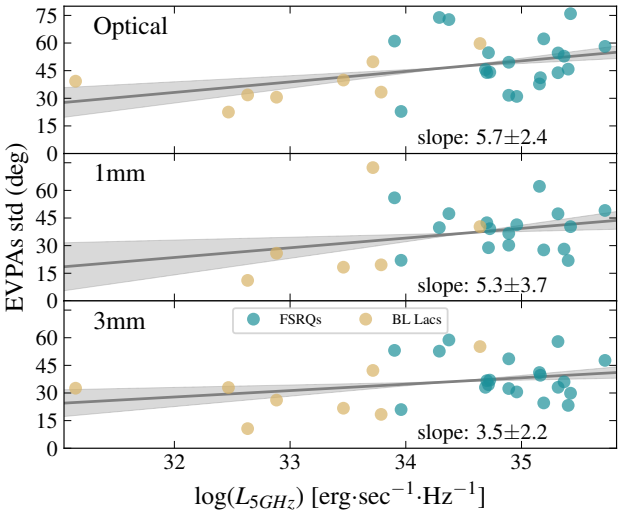

Figure 3. EVPAs spread in three bands as a function of radio luminosity. The gray line and the shadow area represent the best linear fit using a least-squares fitting method and the 1σ deviation, respectively.

Recent results from the Imaging X-ray Polarimetry Explorer (A. P. Marscher et al. 2024) suggest the "energy-stratified" model as the best framework for explaining the polarimetric behavior of blazars across the optical to X-ray bands. In this model, relativistic particles in jets are accelerated in the proximity of the front of shock waves that are either stationary (recollimation shocks) or travel along the jet (A. Sciaccaluga et al. 2025). As shock-accelerated particles propagate downstream, they undergo progressive cooling, primarily via synchrotron and Compton radiation. This leads to the energy stratification of electrons as they travel away from the acceleration site. In addition, shock compression is expected to amplify the magnetic-field component parallel to the shock front, and therefore to have a magnetic field that is partially ordered. One thus expects a higher degree of polarization at

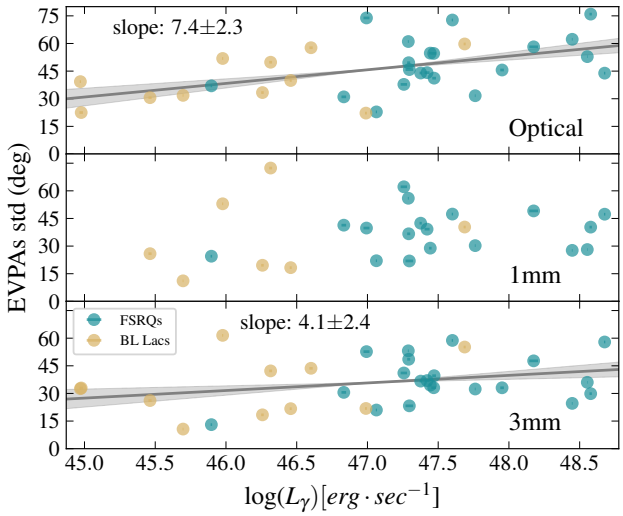

Figure 4. EVPAs spread in three bands as a function of gamma-ray luminosity. The gray line and shadow area are as in Figure 3.

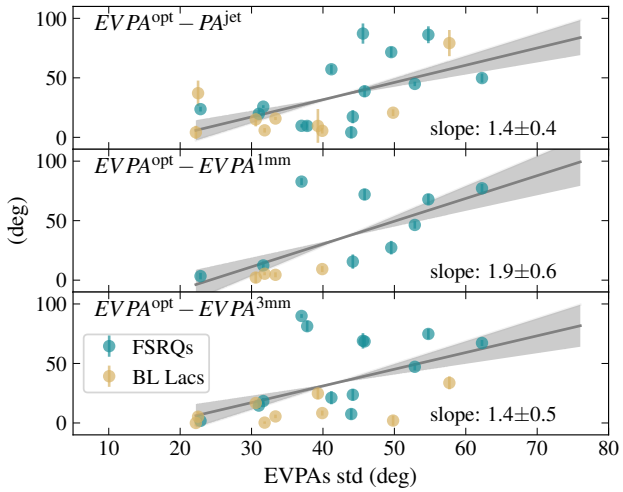

Figure 5. The optical EVPA spread in function of the alignment between the optical EVPA and the jet PA (upper panel), the 1 mm EVPAs (middle panel), and the 3 mm EVPAs (bottom panel). The optical EVPA spread correlates with the divergence between optical EVPAs and the three quantities explored in the three panels. The gray line and the shadow area represent the best linear fit using a least-squares fitting method and the 1σ deviation, respectively.

high frequency, close to the shock front, and lower at low frequencies, further down where the magnetic field becomes more turbulent.

This model may account for the frequency dependence of the degree of polarization, as well as the negative correlation found between EVPA spread and ν_{SP} in the optical domain (Figure 2). The same correlation was, in fact, found in a different sample of blazars using optical polarimetric data from the Robopol program (E. Angelakis et al. 2016), and it was explained by accounting for distinct locations for the optical emission in low- (LSP; $\log(\nu_{SP}) < 14$) and high-synchrotron-peaked (HSP; $\log(\nu_{SP}) > 15$) blazars. In LSP sources, such as FSRQs and low-frequency peaked BL Lac objects, the optical emission probes the high-energy end of the synchrotron spectrum, which typically peaks in the near-infrared. According to the energy-stratified model, the optical emission in these sources originates from a compact region close to the shock

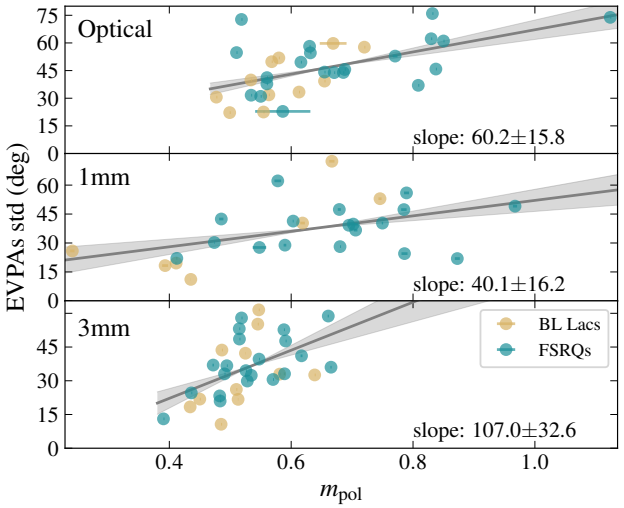

Figure 6. Intrinsic modulation index of fractional polarization versus the standard deviation of EVPA in the corresponding band.

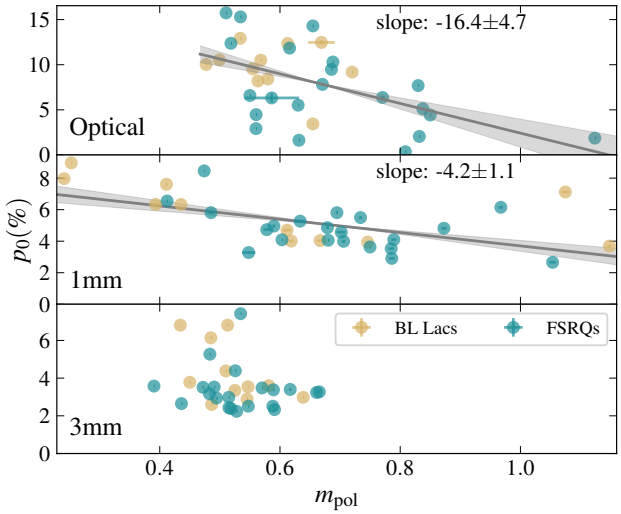

Figure 7. Intrinsic average fractional polarization versus the intrinsic modulation index of polarization in the same band.

front, where higher and faster variability is expected both in total and linearly polarized emission. In contrast, in HSP blazars, the optical emission corresponds to the low-energy end of the synchrotron component and thus arises further downstream from the particle-accelerated site, where the magnetic field is more stable. However, the same qualitative explanation is hard to reconcile with the EVPA spread–$\nu_{\rm SP}$ correlation found also at millimeter waves, since millimeter-wave emission comes from the low-energy part of the synchrotron spectrum in both spectral classes.

The correlations between EVPA spread and $\nu_{\rm SP}$, at both optical and millimeter waves, can be interpreted in an alternative energy-stratified model, where the stratification results from magnetic reconnection in a turbulent environment (B. de Jonge et al. 2026). Electrons close to and above $\nu_{\rm SP}$ concentrate in small parts of plasmoids or plasmoid mergers, where the magnetic field can be very ordered, leading to high p_0 and low $m_{\rm pol}$. Such small regions evolve rapidly: electrons can quickly move to other parts of plasmoids and mergers, where the field lines are ordered in a different direction (H. Zhang et al. 2018). This can result in large EVPA spreads or even angle rotations. By contrast, electrons below $\nu_{\rm SP}$ occupy most of the plasmoid volume and represent its homogeneous component. This results in low p_0 and small EVPA spread (H. Zhang et al. 2024). In summary, for a given synchrotron peak frequency, the average p_0 and EVPA spread rise with the electron energy. The above scenario naturally explains the anticorrelations between EVPA spread and $\nu_{\rm SP}$, as well as between p_0 and $m_{\rm pol}$ at all wavelengths. However, this model predicts an anticorrelation between p_0 and $\nu_{\rm SP}$, which is not observed in this study, and it does not reproduce the higher p_0 values of BL Lacs compared to FSRQs.

The multiband EVPA spread–$\nu_{\rm SP}$ anticorrelation may also indicate a more ordered global magnetic-field geometry in low-power sources compared to high-power ones. Given the known anticorrelation between jet power and $\nu_{\rm SP}$ in blazars, the EVPA spread–$\nu_{\rm SP}$ anticorrelation translates into a positive correlation of EVPA spread with the jet power, here represented by the radio and gamma-ray luminosities (Figures 3 and 4). In the jet emission model proposed by W. J. Potter & G. Cotter (2015), high-power blazars (FSRQs) exhibit jets that accelerate over longer distances, achieving

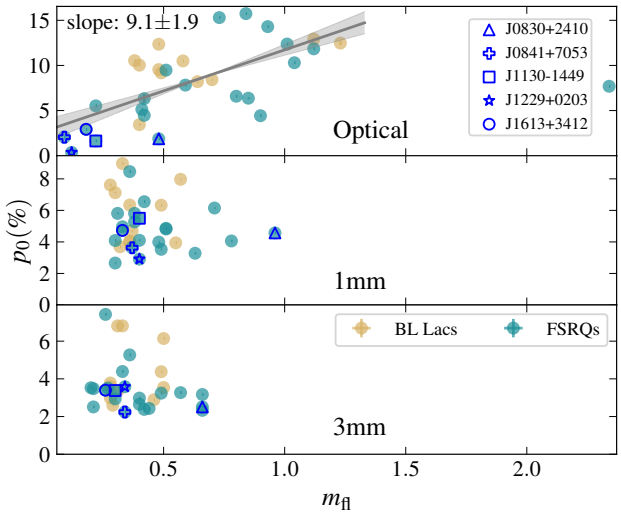

Figure 8. Intrinsic modulation index of the flux density versus the intrinsic average polarization in the corresponding band. The outlier (CTA102 aka J2232+1143) in the optical panel is not taken into account in the fitting procedure.

higher asymptotic Lorentz factors and larger transition radii. The transition radius marks the point where the jet reaches equipartition and transits from an accelerated to a freely expanding geometry. The bulk of the synchrotron emission is expected to originate at the transition region, where the jet attains its maximum Lorentz factor. Given the larger transition radii, in FSRQs the transition region spans a larger area, resulting in a lower magnetic-field strength and, consequently, a lower $\nu_{\rm SP}$. This model would then explain the anticorrelation between jet power and $\nu_{\rm SP}$ found in blazars. Additionally, larger transition radii encompass a broader range of magnetic-field orientations, which may account for the lower fractional polarization and larger EVPA spread observed in FSRQs in this study. However, this model fails to provide a satisfactory explanation for the high $m_{\rm pol}$ observed in these sources.

We have examined the behavior of sources with very low optical fractional polarization, $p_0 \leqslant 3\%$, which are also marked in Figure 8. Differently, at millimeter wavelengths, these sources

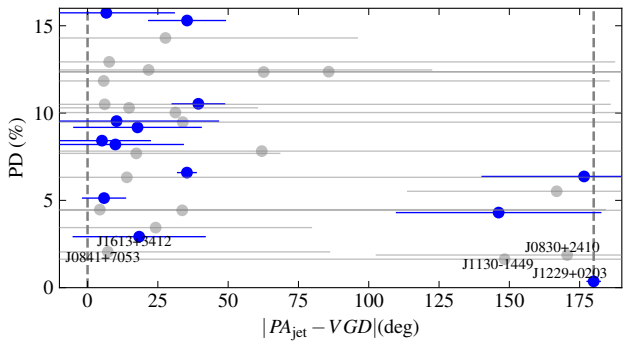

Figure 9. Dependence of optical fractional polarization on the angle between the jet position angle and the VLBI-to-Gaia displacement vector.

have $p_0 \geqslant 2\%$. As explained in Section 3.3, the unusually low degree of polarization in the optical band can either hint at a more turbulent magnetic field in the optical-emitting region or at a significant contribution to the optical emission from the unbeamed or thermal components, like the accretion disk, BLR, or torus. From Figure 8, we learn that sources with low optical p_0 tend to vary less in flux density, which could be explained if the optical emission comes from a nonbeamed component. The optical m_{pol} and EVPA spreads instead cover a wide range of values, from 0.6 to 1.1 for m_{pol}, and from 37° to 76° for the EVPA spread, or even EVPAs uniformly distributed, as is the case of J1130-1449. To investigate the possible contribution of the disk, or BLR, typically located upstream of the millimeter-wave-emitting region, we inspected the very long baseline interferometry (VLBI)–Gaia offsets for the POLAMI sources, taking values from D. Blinov & A. Arshinova (2024). The milliarcsecond precision in optical astrometry provided by the European Space Agency's (ESA) Gaia mission (Gaia Collaboration et al. 2016) led to the discovery of AGN exhibiting significant positional offsets between radio VLBI and Gaia measurements, with amplitudes reaching tens of milliarcseconds (e.g., L. Petrov & Y. Y. Kovalev 2017). It was found that in jetted AGN, the VLBI-to-Gaia displacements (VGDs) tend to align with the direction of the radio jet. Moreover, jetted AGN with Gaia positions located upstream of the VLBI coordinates, hence toward the disk/BLR region, exhibit lower optical polarization than their downstream counterparts, as expected if disk or BLR dominate the optical emission (Y. Y. Kovalev et al. 2020; D. Blinov & A. Arshinova 2024).

In D. Blinov & A. Arshinova (2024), the VGD is parameterized by the angle between the VLBI jet direction and the vector connecting the VLBI and Gaia positions. In this way, the 0° and 180° angles represent sources with Gaia positions downstream and upstream of the VLBI coordinates, respectively. We adopted the definition of the uncertainty on the VGD angle from D. Blinov & A. Arshinova (2024), but reduced its value by half, as the original values refer to 2σ positional errors and may therefore be overestimated. The VGDs for the POLAMI sources are shown against their mean optical fractional polarization in Figure 9. Sources with VGD uncertainties >90° are marked in gray. We noted a bimodal distribution in VGD, around 0° and 180°, in agreement with previous studies (Y. Y. Kovalev et al. 2020; D. Blinov & A. Arshinova 2024). Interestingly, of the five sources with $p_0 \leqslant 3\%$ (see Figure 8), three have VGDs close to 180°. There is also a clear lack of sources with high polarization and upstream offsets. All this may support the hypothesis of a strong contribution from the accretion disk or BLR to both the total and linearly polarized emission at optical frequencies.

K. E. Williamson et al. (2014) reached similar conclusions from the analysis of optical spectral indices over different periods of activity of the sources. In particular, they found a flattening of the optical spectra of FSRQs during quiescent states, but not in BL Lacs. This suggests a dominant disk contribution in optical emission in FSRQs during quiescent states. Notably, the three sources mentioned above, which display low p_0 and VGDs close to 180°, also show low m_{fl}, suggesting a dominance of quiescent states. However, the contribution from the accretion disk is well documented in only one of the three sources, J1229+0203. According to Y.-R. Li et al. (2020), the jet accounts for only 10%–40% of the optical emission in this source, depending on the brightness state.

4.2. The Magnetic-field Structure

Of the six sources with 3 mm EVPAs stable around the mean for at least 70% of their time, three (J1229+0203, J1256-0547, and J2202+4216) show either a zig-zag pattern in their jet profiles (E. V. Kravchenko et al. 2025) or a filamentary structure in both total and polarized emission, with consequent variations of EVPA orientations along the filaments (A. P. Lobanov & J. A. Zensus 2001; A. Fuentes et al. 2023; D.-W. Kim et al. 2023). The stability of 3 mm EVPAs suggests that integrated values of the fractional polarization, as measured by the POLAMI program, are markers of the bulk magnetic field and are not affected by local perturbations.

Several sources have shown evidence of toroidal or helical magnetic field geometries in previous studies: J0854+2006 (J. L. Gómez et al. 2022), J1229+0203 (T. Hovatta et al. 2012), J1256-0547 (A. Fuentes et al. 2023), J2202+4216 (J. L. Gómez et al. 2016), and J2232+1143 (C. Casadio et al. 2019). Of the above sources, J0854+2006, J1256-0547, and J2202+4216 show alignment of EVPAs among frequencies and with the jet PA, in agreement with the expected helical magnetic field geometry. In the two remaining sources, J1229+0203 and J2232+1143, millimeter EVPAs are instead almost perpendicular to the jet PA and deviate from optical EVPA directions. T. Hovatta et al. (2019) found a very high Faraday rotation measure (RM) of $(5.0 \pm 0.3) \times 10^5$ rad m^{-2} at 1 mm in the jet of J1229+0203, leading to an EVPA rotation of ∼30°. Even considering the large rotation affecting 1 mm EVPAs, this could not account for the almost 90° difference between millimeter and optical EVPAs or millimeter EVPAs and jet PA. This implies that millimeter EVPAs, as measured within POLAMI, do not trace the overall helical magnetic-field geometry in this source. The polarized emission at millimeter waves could be dominated by a bright feature observed downstream of the 3 mm core, as observed in C. Casadio et al. (2017). The discrepancy between optical and millimeter EVPAs is additional evidence supporting a disk/BLR contribution to the optical emission.

5. Summary and Conclusions

We present a systematic study of a blazar sample, comparing optical and millimeter-wavelength polarimetric data from 15 yr of observations. This work was carried out within the framework of the POLAMI program, which defined the source sample (21 FSRQs, 11 BL Lacs, and 2 radio galaxies) and provided polarimetric data at 1 and 3 mm from

2006 October to 2021 October. These data were complemented with optical photopolarimetric data obtained from several telescopes (see Section 2), covering the period from 2005 April to 2021 September. The main results can be summarized as follows:

1. The average fractional polarization increases with observing frequency.
2. On average, BL Lacs have higher fractional polarization than FSRQs.
3. 67% of FSRQs and 82% of BL Lacs have EVPAs following a nonuniform distribution. The EVPAs in both radio galaxies instead follow a uniform distribution.
4. EVPAs in BL Lacs are less variable (i.e., have a smaller spread) than in FSRQs at all three bands. In the majority of BL Lacs, EVPAs tend to align across bands, whereas in FSRQs, this occurs in the minority of sources.
5. The larger the spread in optical EVPAs, the greater the deviation between optical and millimeter-wave EVPAs, as well as between optical EVPA and the jet PA.
6. The EVPA spread at the three frequencies anticorrelates with the synchrotron peak frequency.
7. Of the five sources with a low degree of polarization ($<3\%$) and low flux density variability in optical, three of them have Gaia positions upstream of the VLBI radio core.

The above findings are in good agreement with the model proposed by W. J. Potter & G. Cotter (2015), where the contrasting observational properties of FSRQs and BL Lacs are attributed to differences in accretion rate, and consequently in jet power. High-power sources can propagate to larger distances before reaching equipartition, resulting in larger jet radii at the transition regions compared to low-power sources. In this framework, and considering the above findings, the millimeter and optical emissions arise from a larger jet section in FSRQs than in BL Lacs, with consequently lower magnetic-field strength that would lead to a lower synchrotron peak frequency, lower degree of polarization, and larger spread in EVPA orientation, as we observe in this study.

The observed positive correlation of polarization degree with frequency indicates an increasing compactness of the emitting region with frequency. This, and some of the observed correlations in polarization, may also be explained within an energy-stratified model in a turbulent environment, where the stratification arises from magnetic reconnection (e.g., B. de Jonge et al. 2025). Alternatively, similar behavior could result from turbulence (A. P. Marscher 2014) in an energy-stratified shock-in-jet model (I. Liodakis et al. 2022). It is likely that a hybrid approach, incorporating models that address both macro- and microscale processes, offers the most realistic representation.

Additionally, we find that some of the sources with low optical fractional polarization (all FSRQs) show strong evidence that the optical and millimeter-wave emission are not cospatial, with the optical emission likely having a significant contribution from the accretion disk and/or BLR.

Acknowledgments

The POLAMI observations were carried out at the IRAM 30 m Telescope. IRAM is supported by INSU/CNRS (France), MPG (Germany), and IGN (Spain). Some of the optical data analyzed in this paper were collected at the Centro Astronómico Hispano en Andalucía (CAHA), which is operated jointly by Junta de Andalucía and Consejo Superior de Investigaciones Científicas (IAA-CSIC). This study makes use of VLBA data from the VLBA-BU Blazar Monitoring Program (BEAM-ME and VLBA-BU-BLAZAR; http://www.bu.edu/blazars/BEAM-ME.html), funded by NASA through the Fermi Guest Investigator Program. The VLBA is an instrument of the National Radio Astronomy Observatory. The National Radio Astronomy Observatory is a facility of the National Science Foundation operated by Associated Universities, Inc. This study used observations conducted with the 1.8 m Perkins Telescope Observatory (PTO) in Arizona (USA), which is owned and operated by Boston University. The Liverpool Telescope is operated on the island of La Palma by Liverpool John Moores University in the Spanish Observatorio del Roque de los Muchachos of the Instituto de Astrofisica de Canarias with financial support from the UK Science and Technology Facilities Council. C.C., D.B., and D. A. acknowledge support from the European Research Council (ERC) under the Horizon ERC Grants 2021 program under the grant agreement No. 101040021. The IAA-CSIC coauthors, C. C. and D.B., acknowledge financial support from the Spanish "Ministerio de Ciencia e Innovación" (MCIN/AEI/10.13039/501100011033) through the Center of Excellence Severo Ochoa award for the Instituto de Astrofísica de Andalucía-CSIC (CEX2021-001131-S), and through grants PID2019-107847RB-C44 and PID2022-139117NB-C44. The research at Boston University was supported in part by National Science Foundation grant AST-2108622 and by NASA Fermi Guest Investigator grants 80NSSC23K1507 and 80NSSC23K1508 (and their predecessors). H.Z. is supported by NASA under award No. 80GSFC24M0006 and also IXPE GO program Cycle 1, grant Nos. 80NSSC24K1160 and 80NSSC24K1173.

Author Contributions

C.C. and D.B. were responsible for writing the manuscript and analyzing the data. I.A. conceived the research goals and led the POLAMI program. I.A., C.C., I.M., C.T., J.E.P., and D.A-O. were responsible for proposal writing, observations, and data calibration for the POLAMI program. S.J., A.M., M. J., and Z.R.W. were responsible for data acquisition from the Perkins Telescope and contributed to the scientific discussion underlying the study. H.Z. contributed to the scientific discussion and edited the manuscript. C.M.C., H.J., and I.A. S. were responsible for the acquisition and analysis of data from the Liverpool Telescope. G.A.B., T.S.G., E.G.L., D.A. M., S.S.S., I.S.T., Y.V.T., and A.A.V. were responsible for the acquisition, calibration, and analysis of data from the Crimean Astrophysical Observatory and the LX-200 Telescope of St. Petersburg University.

ORCID iDs

Carolina Casadio https://orcid.org/0000-0003-1117-2863
Dmitry Blinov https://orcid.org/0000-0003-0611-5784
Iván Agudo https://orcid.org/0000-0002-3777-6182
Ioannis Myserlis https://orcid.org/0000-0003-3025-9497
Clemens Thum https://orcid.org/0009-0006-5292-6974
Svetlana Jorstad https://orcid.org/0000-0001-6158-1708
Alan Marscher https://orcid.org/0000-0001-7396-3332
Haocheng Zhang https://orcid.org/0000-0001-9826-1759

Juan Escudero Pedrosa https://orcid.org/0000-0002-4131-655X
Diego Álvarez-Ortega https://orcid.org/0000-0002-9998-5238
Zachary R. Weaver https://orcid.org/0000-0001-6314-0690
Manasvita Joshi https://orcid.org/0000-0003-1134-7352
Callum McCall https://orcid.org/0000-0002-3375-3397
Helen Jermak https://orcid.org/0000-0002-1197-8501
Iain A. Steele https://orcid.org/0000-0001-8397-5759
George A. Borman https://orcid.org/0000-0002-7262-6710
Tatiana S. Grishina https://orcid.org/0000-0002-3953-6676
Elena G. Larionova https://orcid.org/0000-0002-2471-6500
Daria A. Morozova https://orcid.org/0000-0002-9407-7804
Sergey S. Savchenko https://orcid.org/0000-0003-4147-3851
Ivan S. Troitskiy https://orcid.org/0000-0002-4218-0148
Yulia V. Troitskaya https://orcid.org/0000-0002-9907-9876
Andrey A. Vasilyev https://orcid.org/0000-0002-8293-0214

References

Abdollahi, S., Acero, F., Baldini, L., et al. 2022, ApJS, 260, 53
Agudo, I., Molina, S. N., Gómez, J. L., et al. 2012, IJMPS, 8, 299
Agudo, I., Thum, C., Molina, S. N., et al. 2018b, MNRAS, 474, 1427
Agudo, I., Thum, C., Ramakrishnan, V., et al. 2018a, MNRAS, 473, 1850
Ajello, M., Angioni, R., Axelsson, M., et al. 2020, ApJ, 892, 105
Angelakis, E., Hovatta, T., Blinov, D., et al. 2016, MNRAS, 463, 3365
Arnold, D. M., Steele, I. A., Bates, S. D., Mottram, C. J., & Smith, R. J. 2012, SPIE, 8446, 84462J
Blandford, R. D., & Znajek, R. L. 1977, MNRAS, 179, 433
Blinov, D., & Arshinova, A. 2024, A&A, 691, A35
Blinov, D., Jorstad, S. G., Larionov, V. M., et al. 2021a, MNRAS, 505, 4616
Blinov, D., Kiehlmann, S., Pavlidou, V., et al. 2021b, MNRAS, 501, 3715
Blinov, D., Pavlidou, V., Papadakis, I., et al. 2018, MNRAS, 474, 1296
Blinov, D., Pavlidou, V., Papadakis, I. E., et al. 2016, MNRAS, 457, 2252
Böttcher, M., van Soelen, B., Britto, R. J., et al. 2017, Galax, 5, 52
Casadio, C., Gómez, J. L., Jorstad, S. G., et al. 2015, ApJ, 813, 51
Casadio, C., Krichbaum, T. P., Marscher, A. P., et al. 2017, Galax, 5, 67
Casadio, C., Marscher, A. P., Jorstad, S. G., et al. 2019, A&A, 622, A158
de Jonge, B., Zhang, H., Errando, M., Gokus, A., & Rabinowitz, P. 2026, ApJ, 997, 360
Fuentes, A., Gómez, J. L., Martí, J. M., et al. 2023, NatAs, 7, 1359
Gaia Collaboration, Prusti, T., de Bruijne, J. H. J., et al. 2016, A&A, 595, A1
Ghisellini, G., Celotti, A., Fossati, G., Maraschi, L., & Comastri, A. 1998, MNRAS, 301, 451
Gómez, J. L., Lobanov, A. P., Bruni, G., et al. 2016, ApJ, 817, 96
Gómez, J. L., Traianou, E., Krichbaum, T. P., et al. 2022, ApJ, 924, 122
Hovatta, T., Lister, M. L., Aller, M. F., et al. 2012, AJ, 144, 105
Hovatta, T., O'Sullivan, S., Martí-Vidal, I., Savolainen, T., & Tchekhovskoy, A. 2019, A&A, 623, A111
Itoh, R., Nalewajko, K., Fukazawa, Y., et al. 2016, ApJ, 833, 77
Jorstad, S. G., Marscher, A. P., Stevens, J. A., et al. 2007, AJ, 134, 799
Kim, D.-W., Janssen, M., Krichbaum, T. P., et al. 2023, A&A, 680, L3
Kovalev, Y. Y., Zobnina, D. I., Plavin, A. V., & Blinov, D. 2020, MNRAS, 493, L54
Kravchenko, E. V., Pashchenko, I. N., Homan, D. C., et al. 2025, MNRAS, 538, 2008
Kudryavtsev, D. O., Sotnikova, Y. V., Stolyarov, V. A., et al. 2024, RAA, 24, 055011
Li, Y.-R., Zhang, Z.-X., Jin, C., et al. 2020, ApJ, 897, 18
Liodakis, I., Marscher, A. P., Agudo, I., et al. 2022, Natur, 611, 677
Lobanov, A. P., & Zensus, J. A. 2001, Sci, 294, 128
Marscher, A. P. 2014, ApJ, 780, 87
Marscher, A. P., Di Gesu, L., Jorstad, S. G., et al. 2024, Galax, 12, 50
Marscher, A. P., & Jorstad, S. G. 2021, Galax, 9, 27
Marscher, A. P., Jorstad, S. G., Larionov, V. M., et al. 2010, ApJL, 710, L126
McKinney, J. C. 2006, MNRAS, 368, 1561
Pacholczyk, A. G. 1970, Radio Astrophysics. Nonthermal Processes in Galactic and Extragalactic Sources (W. H. Freeman)
Padovani, P., Alexander, D. M., Assef, R. J., et al. 2017, A&ARv, 25, 2
Petrov, L., & Kovalev, Y. Y. 2017, MNRAS, 471, 3775
Pichel, A., Donzelli, C., Muriel, H., et al. 2023, A&A, 680, A52
Podjed, S. A., Hickox, R. C., Isler, J. C., Böttcher, M., & Schutte, H. M. 2024, ApJ, 968, 130
Potter, W. J., & Cotter, G. 2015, MNRAS, 453, 4070
Raiteri, C. M., Villata, M., Acosta-Pulido, J. A., et al. 2017, Natur, 552, 374
Richards, J. L., Hovatta, T., Max-Moerbeck, W., et al. 2014, MNRAS, 438, 3058
Richards, J. L., Max-Moerbeck, W., Pavlidou, V., et al. 2011, ApJS, 194, 29
Sasada, M., Jorstad, S., Marscher, A. P., et al. 2018, ApJ, 864, 67
Schlafly, E. F., & Finkbeiner, D. P. 2011, ApJ, 737, 103
Sciaccaluga, A., Costa, A., Tavecchio, F., et al. 2025, A&A, 699, A296
Singal, J., Ko, A., & Petrosian, V. 2014, ApJ, 786, 109
Urry, C. M., & Padovani, P. 1995, PASP, 107, 803
Vaillancourt, J. E. 2006, PASP, 118, 1340
Véron-Cetty, M. P., & Véron, P. 2010, A&A, 518, A10
Weaver, Z. R., Jorstad, S. G., Marscher, A. P., et al. 2022, ApJS, 260, 12
Williamson, K. E., Jorstad, S. G., Marscher, A. P., et al. 2014, ApJ, 789, 135
Zhang, H., Dong, L., & Giannios, D. 2024, MNRAS, 531, 4781
Zhang, H., Li, X., Guo, F., & Giannios, D. 2018, ApJL, 862, L25